# PnuTac: A vision-based pneumatic tactile sensor for slip detection and object classification

Prasad Rayamane[1], Peter Herbert[2], Francisco Munguia-Galeano[1] and Ze Ji[1]

***Abstract*— Soft optical tactile sensors allow robots to capture important information, such as contact geometry, estimations of object compliance, and slip detection. However, most optical tactile sensors utilize gel-filled elastic membranes with non-variable stiffness. To overcome this limitation, this paper presents the development of a pneumatic tactile sensor with tunable pressure (PnuTac). The sensor comprises a pneumatic system, an elastic membrane, and a sealed chamber with a camera inside. The inner side of the membrane layer has dot markers on its surface that are used for slip detection. Slippage is prevented by controlling a Robotiq 2-finger gripper that closes according to the slip detection signal. Additionally, objects held by the gripper appear as contours in sensor images. A dataset of 10,000 such images from 10 tools was utilized for training a VGG-19 convolutional neural network for tool classification. Our results show that increasing the pressure of the PnuTac sensor reduces the time it takes for the gripper to stabilize a slipping object. The trained neural network, fed from the PnuTac's sensor live data, successfully classified 8 out of the 10 tools.**

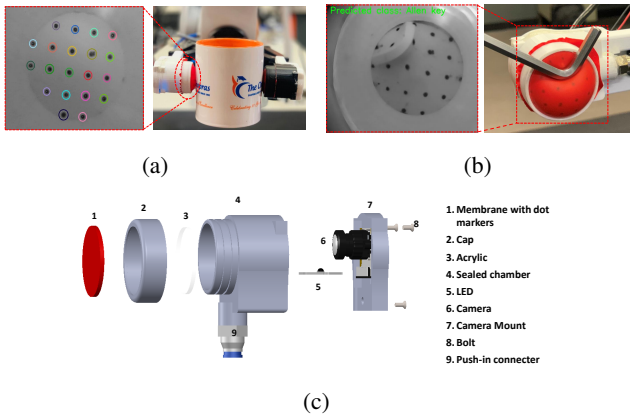


Fig. 1: PnuTac: Vision-based pneumatic optical tactile sensor. (a) Slip detection. (b) Object classification (c). Exploded view of the PnuTac sensor.

## I. Introduction

Tactile sensing allows robots to make informed decisions about how to handle objects based on their shapes and textures [1], [2]. One of the most relevant applications of tactile sensing is detecting whether a robot has securely grasped an object [3], [4]. In this context, a common cause of grip failure is slippage. Humans recognize slipping based on the subtle vibrations of a sliding object and the skin-stretching feeling of their fingertips. However, robots require the assistance of tactile sensors to detect slippage effectively [5].

For a long time, researchers have worked towards developing tactile sensors that can detect slippage based on contact forces, oscillations, accelerations, and surface strain. For example, Su et al. [6] and Ajoudani et al. [7] proposed grasping control systems with slip-detection capabilities based on vibration measurement. The systems enable robots to adjust the grip force based on the detected slip conditions, leading to a more stable grasp. However, these approaches are based on biomimetic and force/torque sensors and lack the classification capabilities that humans possess to identify what they are touching.

Aiming to overcome this issue, vision-based tactile sensors (VBTS) have been proposed as a low-cost alternative that, from the point of view of image processing, the image features can be used not only to analyze force and slip but also for object classification [8]. There are several works that propose different designs of VBTS, such as GelSight [9], DIGIT [10], Omnitact [11], DotView [12], and DelTact [13]. Notably, these sensors have shown robustness and proved to be of low-cost manufacture. However, the use of pneumatic systems and the potential improvements this characteristic may bring to robotic manipulation have not been explored. Additionally, the aforementioned works lack methodologies for training neural networks from the VBTS images for classification purposes.

This paper proposes a new design for a pneumatic-based optical tactile sensor (PnuTac[1]), aiming to address the knowledge gaps of previous works. The PnuTac comprises a pneumatic system, an elastic membrane, and a sealed chamber with a camera inside (Fig. 1c). The inner side of the membrane layer has a grid of circular markers on its surface that are used for slip detection. The experiments to validate the PnuTac sensor include using its slip detection capacity to control a gripper to prevent the slippage of three different objects, two of which involve variable weight. Objects held by the gripper appear as contours in sensor images. A dataset of 10,000 such images from 10 tools was utilized for training a VGG-19 convolutional neural network for tool classification. The contributions of this work can be summarized as follows: (i) the design of a vision-based pneumatic optical tactile sensor with tunable pressure, (ii) the development of a framework based on the PnuTac sensor for slip detection (Fig. 1a) and object classification (Fig. 1b).

[1]https://youtu.be/HJ_ZX18Tw8Y

[1]Prasad Rayamane, Francisco Munguia-Galeano, and Ze Ji with the School of Engineering, Cardiff University, Cardiff, CF24 3AA, United Kingdom {RayamanePB, MunguiaGaleanoF, jiz1}@cardiff.ac.uk

[2]Peter Herbert is with the School of Computer Science and Informatics, Cardiff University, Cardiff, CF24 4AG, United Kingdom HerbertP1@cardiff.ac.uk

The rest of the paper is organized as follows. Section II discusses related work in the context of VBTS sensors, followed by section III that describes the design of the PnuTac sensor. Then, in section IV, the slip detection and object classification framework is presented. Section V introduces the experimental setup and discusses the results. Finally, section VII concludes this paper.

## II. Related Work

This section discusses recent advancements and applications of VBTS, with a particular focus on markerless (GelSight [14]) and marker-based (TacTip [15]) sensors, object classification, and slip detection. GelSight sensors utilize a camera to capture tactile images, providing information about the geometry of the touched surface. Unlike traditional tactile sensors, the main characteristic of GelSight is its resistance to external light variations. In the literature, several works based on GelSight sensors are available. For example, Donlon et al. [16] presented an enhanced version of GelSight by changing the optical path to use a waveguide to route light through the fingertip and a mirror to view the sensor surface from a distance. This modification allows for a more compact wedge-shaped fingertip design suitable for cluttered picking scenarios.

A notable application of VBTS is the one proposed by Li et al. [17], in which a GelSight-style sensor is used to train a robot to perform insertion tasks. Additionally, the paper highlights the application of deep tactile model predictive control and the use of palm-shaped GelSlim sensors for robust manipulation. Following a similar approach, She et al. [18] conducted research on flexible cable manipulation by combining grip and pose controllers based on the cable dynamics extracted from the feedback of a GelSight sensor. Further research has been conducted to extract the dynamics of materials or objects to be manipulated. For example, Huang et al. [19] investigated dynamic tactile sensing by addressing the task of estimating liquid properties. They trained a Gaussian Process Regression model using a small amount of actual data to estimate the liquid properties. However, the solutions presented in these approaches are task-specific because they still require a mathematical model of the object or material to be manipulated. This requirement can be complex to calculate when dealing with various objects or materials instead of just one.

A solution to this problem is the implementation of deep learning techniques, where VBTS has been shown to be compatible with the latter. Consequently, many sensor designs rely on these methods. For instance, tactile material and object classification is an interesting use case for tactile sensors, as demonstrated in [20]. The ResNet18 architecture image classifier has been also utilized to simultaneously train and infer concatenated images that combine depth and infrared images from two VBTS in [21]. Padmanabha et al. [11] performed tactile state estimation for a representative insertion task using OmniTact, a thumb-shaped tactile sensor paired with a ResNet-based neural network. A modified VBTS with a robust sensing surface capable of manipulating hard and sharp objects, as well as performing object classification, was proposed in [22]. Sferrazza et al. [23] propose a system based on green fluorescent particles that are randomly distributed within a soft elastic opaque coating, and deep learning is employed to extract information related to the force applied to the sensor's surface.

In addition, many VBTS are marker-based, designed to track the movement of markers. Since its initial proposal in 2009 based on a dome-shaped version [24], TacTip sensors have evolved into more advanced morphologies. For instance, the Tac-M2 [25] sensor was utilized for in-hand manipulation experiments. One year later, a miniaturized and adapted design [26] was successfully employed as a robotic finger. Despite introducing manufacturing improvements and new surface geometries, these sensors share the same working principle: white pins are printed onto a black membrane, which can then be tracked using computer vision methods. In an effort to extract information from beyond the black membrane, Yamaguchi et al. [27] proposed a VBTS called FingerVision that uses a transparent membrane. However, this membrane allows external illumination variance, resulting in reduced robustness and sensing capabilities. Other approaches utilize markers with multiple colors. As a way of illustration, Lin et al. [28] utilize semi-opaque grids of magenta and yellow markers painted on the top and bottom surfaces of a transparent membrane. The mixture of the two colors is used to detect the 3D displacement of the markers.

An important application of VBTS is slip detection, which plays a vital role in achieving reliable grasping or manipulation. Recent reviews of slip detection technologies and methodologies are provided in [5] and [29]. VBTS for slip detection has primarily been applied in robotics, where researchers have long been exploring the use of VBTS for secure object grasping through the detection of physical signals such as vibration and acceleration. For instance, Su et al. [6] utilized a silicone-made pressure sensor to detect slip by observing abrupt changes in tangential force and vibration in response to normal pressure. Similarly, Ajoudani et al. [7] developed a grasp control system equipped with a slip detection feature, where the ratio of shear force to normal force served as an indicator of the probability of slip. Despite the growing number of VBTS designs, Lambeta et al. [10] highlight several drawbacks related to low resolution, ease of use, and compactness in VBTS technology.

Overall, significant progress has been made in terms of design and the applications of VBTS. However, existing sensors are predominantly gel-based, resulting in fixed stiffness. Consequently, the potential advantages of utilizing tunable pressure for secure grasping applications have not been extensively explored. The novelty of this paper lies in the investigation of a pneumatic system that enables not only measurement but also adjustable control of pressure. Furthermore, the white surface and internal lighting of the sensor facilitate the highlighting of object contours held by the gripper, thereby enabling object classification based on these contours.

## III. Hardware Design

In this section, three goals are suggested as the guidelines for the PnuTac sensor design.

1) Robustness: The sensor should provide reliable information about slippage and object classification.
2) Easy to fabricate: The sensor's parts should be easy to replicate, and the electronic components should be easy to acquire.
3) Easy to use: The sensor should be easy to install, operate and maintain.

By following the design goals, the PnuTac vision-based optical tactile sensor comprises three subsystems: tactile, imaging, and pressurization, as shown in Fig. 1c. The details about the three subsystems are elaborated as follows:

1) **Tactile subsystem**: This subsystem is comprised of an elastic sensing membrane with markers on its internal surface. Since the markers are printed using stencils, a thin layer of permanent black ink is spread over the stencils. Then, the stencils are removed, leaving the markers printed over the membrane surface. The inflated sensing membrane forms a spherical shape. The membrane is made from a 0.5 mm thick latex sheet (Fig. 2b).
2) **Pressurization subsystem**: This subsystem comprises the body of the sensor (made of 3D-printed PLA), an acrylic plate to seal the chamber, a Festo SPTE-P10R-Q4-B-2.5K pressure sensor, an Arduino Uno (controller board), and an Arduino-air module (pump). The PnuTac is connected to the pump through the push-in connector (Fig. 2a). The controller board implements a proportional controller that modulates the airflow from the pump into the sealed chamber. In other words, the controller calculates the current pressure in the sealed chamber based on the pressure sensor and increases or decreases it by using pulse width modulation (PWM).
3) **Imaging subsystem**: This subsystem is comprised of a USB RGB camera with a 180-degree fisheye lens attached to the camera and adjusted to focus on the markers. The camera is held at the bottom of the sealed chamber and positioned 25 mm away from the membrane. Fig. 2b and Fig. 2a show the assembly and cross-sectional view of the sensor prototype, where the position of the camera can be observed.

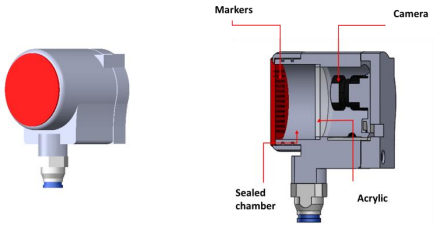


(a) (b)

Fig. 2: PnuTac sensor. (a) Sensor assembly. (b) Cross-sectional view of sensor prototype.

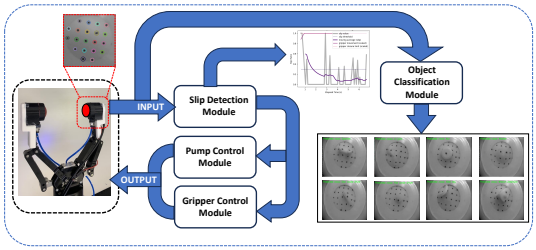


Fig. 3: Slip detection and object classification framework.

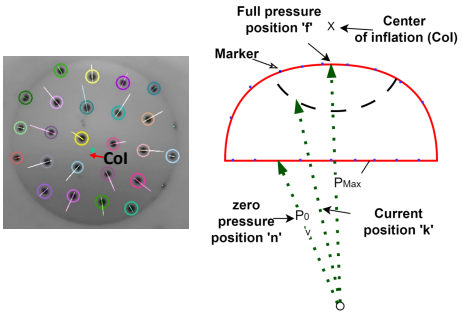


Fig. 4: PnuTac sensor's camera view.

## IV. Framework

This section presents the PnuTac framework for slip detection and object classification (Fig. 3). This comprises the following modules: slip detection, gripper control, pump control and object classification.

The **slip detection module** is responsible for capturing and analyzing images from the pneumatic sensor. As mentioned previously, the sensor consists of a latex membrane with a grid of circular dots imprinted on its internal surface. A fisheye camera captures these dots, and image processing techniques are utilized to track their movement between consecutive frames. The camera is calibrated using the OpenCV library to remove lens distortion.

The undistorted images adhere to the projective pinhole model, indicating that as the dots move away from the camera's image plane perpendicular to it, they generally move outward in the image plane towards a vanishing point. This phenomenon is particularly pronounced due to the camera's short focal length, which influences the perceived movement of the markers. Fig. 7c demonstrates this effect by displaying the optical flow trajectories of the markers as the sensor's elastic membrane is pressurized and inflated. Additionally, the figure illustrates that the center of inflation (CoI), represented by the position vector $\mathbf{c}$, can be estimated through a least squares solution of intersecting lines corresponding to these trajectories. As a result, the CoI serves as a vanishing point for the motion of the dot markers. By knowing the position vector (in the image plane) of the $i^{th}$ marker at both the unpressurized state (denoted as $\mathbf{n_i}$) and the full operating pressure state (denoted as $\mathbf{f_i}$), the cross-ratio identity can be used to calculate the relative height of markers when in a depressed position.

Fig. 5: Objects used for creating the dataset.

$$cross\ ratio = \frac{|\mathbf{f_i} - \mathbf{n_i}||\mathbf{c} - \mathbf{k_i}|}{|\mathbf{f_i} - \mathbf{k_i}||\mathbf{c} - \mathbf{n_i}|} = \frac{|\tilde{\mathbf{f}}_\mathbf{i} - \tilde{\mathbf{n}}_\mathbf{i}|}{|\tilde{\mathbf{f}}_\mathbf{i} - \tilde{\mathbf{k}}_\mathbf{i}|}, \quad (1)$$

where $\mathbf{k_i}$ represents the position vector of the $i^{th}$ marker (in the image plane of a given frame), possibly in a depressed position; and position vectors $\tilde{\mathbf{f}}_\mathbf{i}, \tilde{\mathbf{k}}_\mathbf{i}, \tilde{\mathbf{n}}_\mathbf{i}$ represent the marker position in 3D Euclidean space under the same conditions as the corresponding image plane vectors $\mathbf{f_i}, \mathbf{k_i}, \mathbf{n_i}$, as shown in Fig. 4. In practice, the force applied to the sensor surface cannot be perfectly perpendicular, resulting in some lateral movement that is tangential to the sensor surface. Consequently, the marker position $\tilde{\mathbf{k}}_\mathbf{i}$ may not be collinear with $\mathbf{f_i}$, $\mathbf{n_i}$, and $\mathbf{c}$. Therefore, only the component of $\tilde{\mathbf{k}}_\mathbf{i}$ in the direction of the inflation line (defined by $\mathbf{f_i}$ and $\mathbf{n_i}$) is utilized to calculate the cross-ratio.

The **gripper control module** detects slip events as well as the release and grip actions of the gripper. Inspired by the notion of slip ratio from [30], and given the resolution of the dot grid markers beyond a threshold radius $r_{peri}$ from the CoI were noted as peripheral markers. For experiments, the radius was taken as $r_{peri} = \frac{1}{\sqrt{2}} \times \max(|\mathbf{p_i} - \mathbf{c}|)$. Optical flow vectors $\mathbf{v_i}$ for each marker in a frame were calculated, and a slip ratio value can be calculated by:

$$R = \frac{\max_{\forall i}(\{\mathbf{v}_i \mid |\mathbf{p_i} - \mathbf{c}| \geq r_{peri}\})}{\max_{\forall i}(\{\mathbf{v}_i\})} \quad (2)$$

To reduce the influence of noise when stationary, the slip ratio is detected only when the magnitude of the optical flow vectors exceeds a predetermined threshold (0.1 in the experiments).

The **decision module** can decide if closing the gripper is necessary based on the following:

$$Gripper_{action} = \begin{cases} \text{Grip}, & R > g_{thresh} \\ \text{No action}, & \text{otherwise} \end{cases} \quad (3)$$

where $R$ is the slip ratio, and threshold $g_{thresh}$ determines when the robot gripper should grip the object ($g_{thresh} = 0.3$ in the experiments).

The **pump control module** is responsible for controlling the pressure in the sealed chamber. This module includes functions, such as activating the pump to begin generating pressure, maintaining a near-constant pressure, and adjusting the pressure level based on the feedback from the slip detection module. This module is controlled by the pressurization subsystem introduced in the previous section.

The **object classification module** utilizes a VGG-19 neural network. The images are resized to $224 \times 224$ for the network. The image dataset includes 10,000 images of 10 different objects (Fig. 5) and is split into three sets for training, validation, and testing with proportions of 70%, 10%, and 20%, respectively. Training accuracy reached 97.1%, whilst the validation and test accuracy were 92.1% and 92.6%, respectively. Keras 2.4.0 was used with an Intel Core i5-8400 CPU @ 2.8Ghz with an Nvidia RTX 2080 GPU.

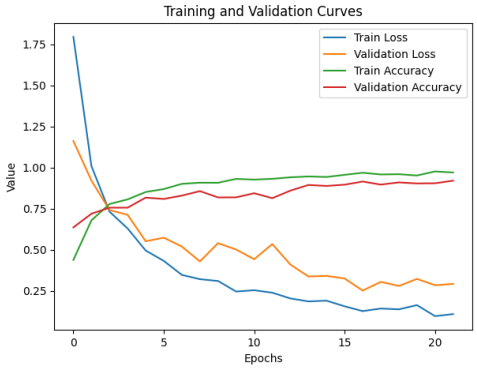


Fig. 6: The learning progress of the object classification module.

## V. Experimental Setup

This section describes the experimental setup utilized to validate the proposed framework. Two series of experiments are performed to evaluate the capabilities of the sensor to detect slippage and its object classification performance in the real world. In the first series of experiments, a KUKA® LBR IIWA 14 robot arm and a Robotiq® 2-finger gripper are utilized. The PnuTac sensor is attached to the gripper's fingers, as shown in Fig. 7. Aiming to investigate whether the slip detection characteristics of the PnuTac sensor lead to a better grip while varying the pressure, the experiments are performed on three different objects: a thermos flask being filled with water (Fig. 7a), an aluminum bar (Fig. 7b) and a cup being filled with granular material (Fig. 7c).

To conduct the experiments, the PnuTac sensor was utilized and tested by setting ten pressure values, as detailed in Table I. For each object, ten trials were attempted for each pressure level, resulting in a total of 100 trials per object for the ten different pressure settings. In total, 300 samples were obtained. Here, every time the system identifies slippage and prevents the object from falling, it is counted as a success and as a failure otherwise, which we refer to as the slip detection success rate. Additionally, the main goal is to investigate the effectiveness of varying the pressure for improving grasp control. Thus, a two-tailed test is performed while taking as a reference $P1$, which is the lowest pressure in Table I. The null hypothesis is formulated as follows: despite the change in pressure, the time that it takes for the gripper to stabilize the object will neither reduce nor increase.

For the second series of experiments, the objects from the dataset are held by the gripper, and the classification module

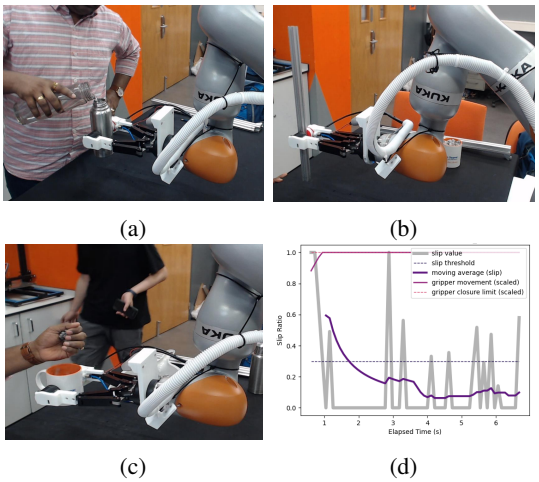


(a) (b) (c) (d)

Fig. 7: Experimental setup. In (a), the robot, using a Robotiq 2-finger gripper with a pneumatic sensor, grips a thermos flask while the user fills water in it. In (b), the robot stabilizes an aluminum bar. In (c), the robot stabilizes a cup. In (d), a graph plotted during a slip detection and prevention experiment is displayed.

is used to predict which object the gripper is holding. If the classification module identifies the object correctly, it is considered a success and a failure otherwise.

| **ID** | P1 | P2 | P3 | P4 | P5 | P6 | P7 | P8 | P9 | P10 |
|---|---|---|---|---|---|---|---|---|---|---|
| **kPa** | 3.4 | 4.1 | 4.8 | 5.5 | 6.2 | 6.8 | 7.5 | 8.2 | 8.9 | 9.6 |

TABLE I: Pressure values used in the experiments.

## VI. Results and Discussion

For the first series of experiments, the slip detection results are analyzed by performing a two-tailed test by comparing all the outcomes against the time it takes for the gripper to stabilize the object while holding, and the PnuTac pressure is equal to $P1$. For each object-pressure pair, the average time it takes for the gripper to stabilize the object is measured. Fig. 7b shows a graph, where the purple line converges to zero after a few seconds, which represent how much the object is slipping. When the purple line crosses the threshold line, the time is stored. The same process was repeated for each pressure-object combination.

For the aluminum profile bar case, the p-values vary from $0.44$ to $0.02$, which follows a trend where the slip time generally decreases as pressure increases, except for P5 and P9, as shown in the table II. For the cup filled with granular material, there is a decrease in time, followed by an increase, and then another decrease as pressure increases, highlighting the non-linear nature of the pressure-slip time relationship. For the case of the thermos filled with water, no consistent decrease or increase in the slip time is observed as the pressure increases.

The aluminum bar, which can be considered a constant load, resulted in easier stabilization. The overall success rate of slip detection for the bar was 91%. In contrast, in the variable load slip detection experiment using a cup filled with granular material, a non-linear behavior was observed due to the variability in the rate of granular fill. Furthermore, when considering the thermos filled with water, it was found that the slip behavior was inconsistent. This inconsistency is attributed to the response of the system trying to close the gripper every time the load changes in order to avoid slippage. The overall success rates for slip detection in the cup filled with granular material and the thermos filled with water were 88% and 82%, respectively.

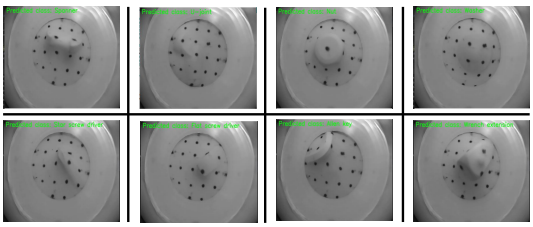

Fig. 8: Predicted classes.

In the second series of experiments, the sensor's performance to identify objects while utilizing the VGG-19 neural network reached 92.6% accuracy on the test dataset, and 8 of the 10 objects were successfully identified from live sensor data. While the sensor successfully identified the spanner, u-joint, extension, nut, washer, star screwdriver, cross screwdriver, and Allen key, as shown in Fig. 8, the sensor, despite trying different positions, could not identify the pliers and the bolt.

## VII. Conclusions

This work presented the design of the PnuTac sensor, which incorporates a pneumatic system to achieve variable pressure. Two experiments were conducted to evaluate the sensor's performance in slip detection with variable pressure inputs. The overall success rate of slip detection was found to be 87%. Additionally, the sensor's performance was validated in terms of object classification by training a neural network on a dataset of 10,000 images representing ten different tools. The results showed that the sensor could classify objects with an accuracy of 80% after training. Overall, the proposed PnuTac sensor demonstrated the potential to detect slippage and, in this way, prevent objects from falling from the gripper. During the experiments, limitations related to objects with variable loads were identified, which proved to be the most challenging scenarios using the PnuTac sensor. However, the reliability of the framework and sensor's slip detection capabilities for both static and variable load objects was demonstrated. Therefore, the implementation of this new sensor has the potential to contribute to safe manipulation tasks.

## References

[1] Ravinder S Dahiya, Giorgio Metta, Maurizio Valle, and Giulio Sandini. Tactile sensing—from humans to humanoids. *IEEE transactions on robotics*, 26(1):1–20, 2009.

| | Case-1 Aluminum Bar | | | | Case-2 Cup | | | | Case-3 Thermos Flask | | | |
|---|---|---|---|---|---|---|---|---|---|---|---|---|
| **Pressure** | **Mean ($\mu$)** | **Standard Deviation ($\sigma$)** | **t-value (10)** | **p-value** | **Mean ($\mu$)** | **Standard Deviation ($\sigma$)** | **t-value (10)** | **p-value** | **Mean ($\mu$)** | **Standard Deviation ($\sigma$)** | **t-value (10)** | **p-value** |
| P1 | 3.84 | 0.80 | | | 3.18 | 1.01 | | | 2.58 | 1.03 | | |
| P2 | 3.56 | 0.71 | 0.79 | 0.44 | 3.05 | 0.78 | 0.25 | 0.81 | 2.51 | 0.90 | 0.15 | 0.88 |
| P3 | 3.36 | 0.78 | 1.29 | 0.22 | 2.64 | 0.70 | 1.45 | 0.17 | 2.38 | 1.03 | -0.17 | 0.87 |
| P4 | 3.42 | 0.87 | 1.07 | 0.30 | 2.67 | 1.12 | 1.12 | 0.29 | 2.60 | 0.08 | -0.66 | 0.52 |
| P5 | 3.79 | 1.08 | 0.11 | 0.91 | 2.83 | 0.85 | 0.95 | 0.36 | 2.39 | 0.83 | -0.11 | 0.92 |
| P6 | 3.35 | 0.73 | 1.36 | 0.19 | 2.83 | 0.85 | 0.94 | 0.36 | 2.43 | 1.02 | 0.24 | 0.81 |
| P7 | 3.04 | 0.44 | 2.62 | 0.02 | 2.87 | 0.62 | 1.39 | 0.20 | 2.42 | 1.02 | -0.94 | 0.37 |
| P8 | 3.06 | 0.33 | 2.72 | 0.02 | 2.77 | 0.84 | 1.06 | 0.31 | 2.42 | 0.81 | -0.18 | 0.86 |
| P9 | 3.46 | 0.88 | 0.96 | 0.95 | 2.62 | 0.71 | 1.07 | 0.31 | 2.43 | 0.52 | 0.79 | 0.45 |
| P10 | 3.07 | 0.48 | 2.49 | 0.02 | 2.56 | 0.92 | 1.05 | 0.32 | 2.66 | 1.00 | 0.00 | 1.00 |

TABLE II: Statistical results from the first series of experiments.


[2] Hanna Yousef, Mehdi Boukallel, and Kaspar Althoefer. Tactile sensing for dexterous in-hand manipulation in robotics—a review. *Sensors and Actuators A: physical*, 167(2):171–187, 2011.

[3] Zhanat Kappassov, Juan-Antonio Corrales, and Véronique Perdereau. Tactile sensing in dexterous robot hands. *Robotics and Autonomous Systems*, 74:195–220, 2015.

[4] Wei Chen, Heba Khamis, Ingvars Birznieks, Nathan F Lepora, and Stephen J Redmond. Tactile sensors for friction estimation and incipient slip detection—toward dexterous robotic manipulation: A review. *IEEE Sensors Journal*, 18(22):9049–9064, 2018.

[5] Maria Teresa Francomano, Dino Accoto, and Eugenio Guglielmelli. Artificial sense of slip—a review. *IEEE Sensors Journal*, 13(7):2489–2498, 2013.

[6] Zhe Su, Karol Hausman, Yevgen Chebotar, Artem Molchanov, Gerald E Loeb, Gaurav S Sukhatme, and Stefan Schaal. Force estimation and slip detection/classification for grip control using a biomimetic tactile sensor. In *2015 IEEE-RAS 15th International Conference on Humanoid Robots (Humanoids)*, pages 297–303. IEEE, 2015.

[7] Arash Ajoudani, Elif Hocaoglu, Alessandro Altobelli, Matteo Rossi, Edoardo Battaglia, Nikos Tsagarakis, and Antonio Bicchi. Reflex control of the pisa/iit softhand during object slippage. In *2016 IEEE International Conference on Robotics and Automation (ICRA)*, pages 1972–1979. IEEE, 2016.

[8] Alexander C Abad and Anuradha Ranasinghe. Visuotactile sensors with emphasis on gelsight sensor: A review. *IEEE Sensors Journal*, 20(14):7628–7638, 2020.

[9] Ian H Taylor, Siyuan Dong, and Alberto Rodriguez. Gelslim 3.0: High-resolution measurement of shape, force and slip in a compact tactile-sensing finger. In *2022 International Conference on Robotics and Automation (ICRA)*, pages 10781–10787. IEEE, 2022.

[10] Mike Lambeta, Po-Wei Chou, Stephen Tian, Brian Yang, Benjamin Maloon, Victoria Rose Most, Dave Stroud, Raymond Santos, Ahmad Byagowi, Gregg Kammerer, et al. Digit: A novel design for a low-cost compact high-resolution tactile sensor with application to in-hand manipulation. *IEEE Robotics and Automation Letters*, 5(3):3838–3845, 2020.

[11] Akhil Padmanabha, Frederik Ebert, Stephen Tian, Roberto Calandra, Chelsea Finn, and Sergey Levine. Omnitact: A multi-directional high-resolution touch sensor. In *2020 IEEE International Conference on Robotics and Automation (ICRA)*, pages 618–624. IEEE, 2020.

[12] Haoran Zheng, Yongbin Jin, Hongtao Wang, and Pei Zhao. Dotview: A low-cost compact tactile sensor for pressure, shear, and torsion estimation. *IEEE Robotics and Automation Letters*, 2023.

[13] Guanlan Zhang, Yipai Du, Hongyu Yu, and Michael Yu Wang. Deltact: A vision-based tactile sensor using dense color pattern. *arXiv preprint arXiv:2202.02179*, 2022.

[14] Micah K Johnson and Edward H Adelson. Retrographic sensing for the measurement of surface texture and shape. In *2009 IEEE Conference on Computer Vision and Pattern Recognition*, pages 1070–1077. IEEE, 2009.

[15] Benjamin Ward-Cherrier, Nicholas Pestell, Luke Cramphorn, Benjamin Winstone, Maria Elena Giannaccini, Jonathan Rossiter, and Nathan F Lepora. The tactip family: Soft optical tactile sensors with 3d-printed biomimetic morphologies. *Soft robotics*, 5(2):216–227, 2018.

[16] Elliott Donlon, Siyuan Dong, Melody Liu, Jianhua Li, Edward Adelson, and Alberto Rodriguez. Gelslim: A high-resolution, compact, robust, and calibrated tactile-sensing finger. In *2018 IEEE/RSJ International Conference on Intelligent Robots and Systems (IROS)*, pages 1927–1934. IEEE, 2018.

[17] Rui Li, Robert Platt, Wenzhen Yuan, Andreas ten Pas, Nathan Roscup, Mandayam A Srinivasan, and Edward Adelson. Localization and manipulation of small parts using gelsight tactile sensing. In *2014 IEEE/RSJ International Conference on Intelligent Robots and Systems*, pages 3988–3993. IEEE, 2014.

[18] Yu She, Shaoxiong Wang, Siyuan Dong, Neha Sunil, Alberto Rodriguez, and Edward Adelson. Cable manipulation with a tactile-reactive gripper. *The International Journal of Robotics Research*, 40(12-14):1385–1401, 2021.

[19] Hung-Jui Huang, Xiaofeng Guo, and Wenzhen Yuan. Understanding dynamic tactile sensing for liquid property estimation. *arXiv preprint arXiv:2205.08771*, 2022.

[20] Huaping Liu, Yupei Wu, Fuchun Sun, and Di Guo. Recent progress on tactile object recognition. *International Journal of Advanced Robotic Systems*, 14(4):1729881417717056, 2017.

[21] Kaiming He, Xiangyu Zhang, Shaoqing Ren, and Jian Sun. Deep residual learning for image recognition. In *Proceedings of the IEEE conference on computer vision and pattern recognition*, pages 770–778, 2016.

[22] Prasad Rayamane, Ze Ji, and Michael Packianather. Design and development of a robust vision-based tactile sensor. In *2022 IEEE/ASME International Conference on Advanced Intelligent Mechatronics (AIM)*, pages 1417–1423. IEEE, 2022.

[23] Carmelo Sferrazza and Raffaello D'Andrea. Design, motivation and evaluation of a full-resolution optical tactile sensor. *Sensors*, 19(4):928, 2019.

[24] Craig Chorley, Chris Melhuish, Tony Pipe, and Jonathan Rossiter. Development of a tactile sensor based on biologically inspired edge encoding. In *2009 International Conference on Advanced Robotics*, pages 1–6. IEEE, 2009.

[25] Benjamin Ward-Cherrier, Luke Cramphorn, and Nathan F Lepora. Tactile manipulation with a tacthumb integrated on the open-hand m2 gripper. *IEEE Robotics and Automation Letters*, 1(1):169–175, 2016.

[26] Benjamin Ward-Cherrier, Nicolas Rojas, and Nathan F Lepora. Model-free precise in-hand manipulation with a 3d-printed tactile gripper. *IEEE Robotics and Automation Letters*, 2(4):2056–2063, 2017.

[27] Akihiko Yamaguchi and Christopher G Atkeson. Combining finger vision and optical tactile sensing: Reducing and handling errors while cutting vegetables. In *2016 IEEE-RAS 16th International Conference on Humanoid Robots (Humanoids)*, pages 1045–1051. IEEE, 2016.

[28] Xi Lin and Michael Wiertlewski. Sensing the frictional state of a robotic skin via subtractive color mixing. *IEEE Robotics and Automation Letters*, 4(3):2386–2392, 2019.

[29] Rocco A Romeo and Loredana Zollo. Methods and sensors for slip detection in robotics: A survey. *Ieee Access*, 8:73027–73050, 2020.

[30] Siyuan Dong, Wenzhen Yuan, and Edward H Adelson. Improved gelsight tactile sensor for measuring geometry and slip. In *2017 IEEE/RSJ International Conference on Intelligent Robots and Systems (IROS)*, pages 137–144. IEEE, 2017.